Open Access

Catalysis Research

LIDSEN Publishing Inc.

Original Research

Leaf Mediated *Curcuma sp.* Silver Nanoparticles as Catalyst - Evaluating Their Antioxidant, Cytotoxicity, Para-Nitrophenol Catalytic and Photocatalytic Activity

Mathivathani Kandiah *, Dharsha Bhaskaran, Ominda Perera

School of Science, BMS, 591, Galle Road Colombo 06, Sri Lanka; E-Mails: mathi@bms.ac.lk; dharsha.bhaskaran@bms.ac.lk; ominda@bms.ac.lk

* **Correspondence:** Mathivathani Kandiah; E-Mail: mathi@bms.ac.lk

Academic Editor: Giane Gonçalves Lenzi

Special Issue: Advance in Photocatalysis

Catalysis Research
2024, volume 4, issue 3
doi:10.21926/cr.2403010

Received: April 29, 2024
Accepted: July 15, 2024
Published: July 22, 2024

Abstract

Nanotechnology is a fast-rising market in catalytic research; however, the production of eco-friendly nanoparticles remains a significant challenge. In this study, silver nanoparticles (AgNPs) were synthesized from the agro-industrial waste of leaves of *C. longa, C. aromatica, C. caesia, C. zedoaria,* and *C. amada* at RT after 24 h, which was confirmed with UV-spectrophotometric evaluation between 320-520 nm. SEM revealed cubic and 30-50 nm AgNPs, while band-gap energy was presented as semi-conductors. Synthesized AgNPs were experimented for their antioxidant, cytotoxic, PNP-catalytic, and photocatalytic activity. The antioxidant assays were determined for WEs and AgNPs. The AgNPs revealed higher TFC, TPC, and TAC than WEs. Cytotoxicity of AgNPs was assessed with the viability of *Artemia salina* and approved to be non-toxic. PNP catalysis was executed with 4000 ppm AgNPs, and remarkable PNP degradation was obtained within 30 minutes. Photocatalytic ability of 4000 ppm and 266.67 ppm AgNPs were tested to degrade methyl-orange, and a rapid degradation was observed with $NaBH_4$. Results of these assays reveal that synthesized AgNPs are potential candidates for integration into the manufacturing of catalytic and photocatalytic agents; thereby, these AgNPs can improve the quality of life by providing cleaner environments for

organisms.

Keywords
Silver nanoparticle; catalysis; photocatalysis; azo-dye; para-nitrophenol

1. Introduction

Catalysis is adding a catalyst to speed up a reaction that is not changed during the chemical reaction. Nanoparticles are considered catalysts due to their high active surface area, modifiable surface properties, and high penetration capability, which can provide an adsorption/desorption site for various reactions [1]. Nanostructures such as silver nanoparticles (AgNPs) are superior to other metal nanoparticles since they have proven less toxic and cost-effective with a high surface plasmon resonance (SPR), which can harness better optical, thermal, electrical, antioxidant, and antimicrobial abilities. Therefore, AgNPs are exploited for several medical, industrial, and environmental bioremediation purposes [2-4].

AgNPs can be synthesized through two major pathways: the bottom-up and top-down approaches. The bottom-up approach exploits green sources or chemicals, while the top-down approach utilizes physical or mechanical processes, as shown in Figure 1 [5]. However, chemical, physical, and mechanical methods produce high expenditures and toxic by-products. In contrast, the green synthesis involves the implementation of phytochemical compounds present in biological sample like the plant extract to be utilized as a reducing agent to reduce Ag^{+} ion of silver salt to Ag^{0} atom which further grows and develops into AgNPs with a cap stabilizing it (Figure 2), therefore the green process aids the current global state with sustainability, eco- friendliness, non-toxicity, and moreover there are plenty of green sources available around various region of the world [6, 7]. Furthermore, water as a solvent for the extraction process provides a high diffusion capability and thermostability of phytochemicals due to polar properties [8].

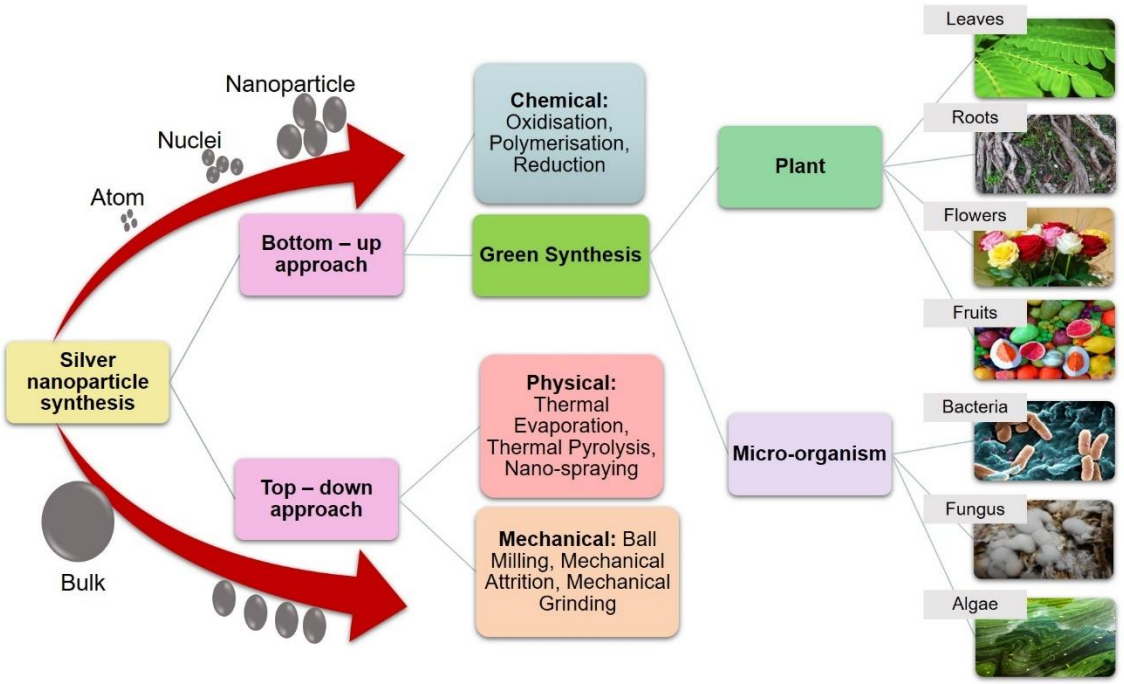

Figure 1 Synthesis of AgNPs, adapted from [5].

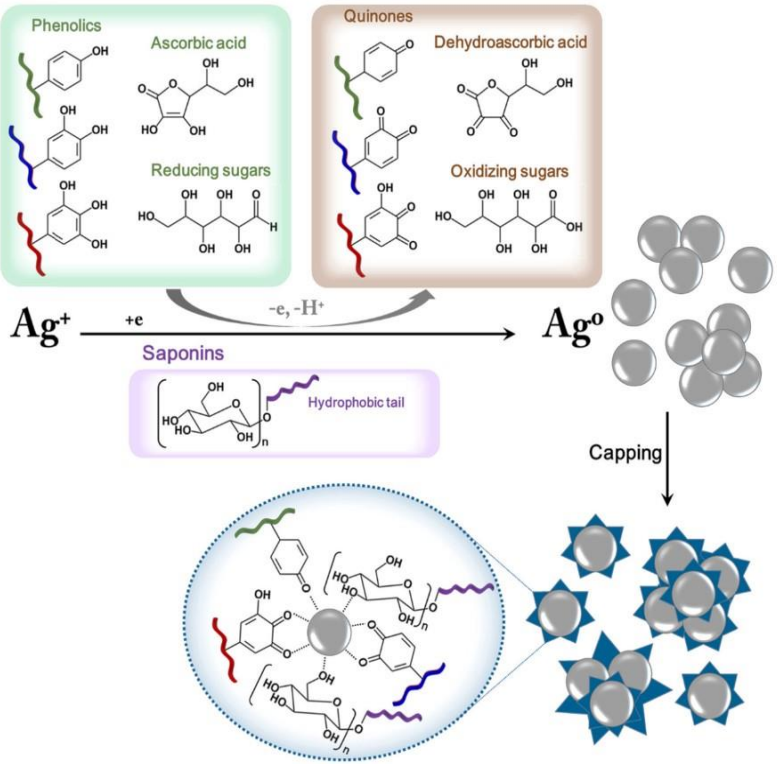

Figure 2 Growth of Ag^+ ion to AgNPs [6].

Additionally, for large-scale AgNP synthesis, the plants are suitable due to their presence of numerous phytochemicals, such as flavonoids and phenols, which can differ according to various species seasons and can be obtained at any location of biodiversity. Therefore, polydisperse AgNPs can be produced. In contrast, microbes are inconvenient due to the biohazards and expenses of handling and culturing [9]. In this study, the leaves of five species belonging to the family of Zingiberaceae and genus *Curcuma* were utilized to synthesize AgNPs. This study also aims to

investigate the possibility of forming AgNP using five different species since the previous research shows that these five species have various levels of similar phytochemicals and other volatile oils [10]. Moreover, *Curcuma* species are well known for their traditional medicine with anti-inflammatory and antibacterial actions due to the presence of potent antioxidants like curcuminoids and are widely consumed in Asia [11]. Million tons of these *Curcuma* plants are mass-produced and harvested for their rhizomes, while their leaves are not widely consumed and are predominantly considered agro-industrial waste, so they can be implemented as a potential raw material for sustainable AgNP synthesis [12].

Since AgNPs are lethal to microbes, it is crucial to determine the cytotoxicity of AgNPs to ensure the safety of the synthesized AgNPs within organisms. Cytotoxicity can result from cell death caused by the accumulation of reactive oxygen species (ROS), which attacks the cell membrane, deoxyribonucleic acid, and protein. This can be tested on AgNPs with a model organism called *Artemia salina* (brine shrimp) to assess their viability, as it is one of the most preferred test organisms exploited in current experiments due to low cost, rapidity, and convenience [13, 14]. Antioxidants can neutralize toxic compounds by scavenging away ROS like $OH^{\bullet}$ and $NO_2^{\bullet}$, which can produce excess oxidative stress [15, 16]. Several studies claim that plant-based AgNPs possess antioxidant ability as they are capped around different types of plants' antioxidants [17, 18].

Environmental and marine pollution can be caused by para-nitrophenol (PNP), a chemical utilized to manufacture dyes, insecticides, explosives, and drugs. PNP is toxic to organisms due to its high stability and solubility in water environments [19]. According to the research [20], the removal of PNP consists of membrane separation and chemical reactions, which are expensive and highly energy-consuming. At the same time, several studies have documented that AgNPs are rapid and affordable catalysts to break down PNP to para-aminophenol (PAP), which supports industrial wastewater remediation [21, 22]. Several industries use azo dye to treat food, textiles, and pharmaceutics. Still, due to their presence of azo bonds, harmful effects are impacted upon ingestion since the bond cleavage forms aromatic amines that are carcinogenic and can harm aquatic organisms [23, 24]. Furthermore, the conventional physical and chemical processes to degrade azo dyes are considered to be inconvenient due to high cost and maintenance [25]. However, studies have utilized AgNPs as a cost-effective photocatalyst due to their high SPR properties [26, 27].

The main aim of this study is to understand the catalytic activity of PNP and photocatalysis of Methyl orange by using the silver nanoparticle synthesized by the extracts of five *Cucurma* species leaves. Furthermore, antioxidant assessments for Total Flavonoid Content (TFC), Total Phenolic Content (TPC), and Total Antioxidant Content (TAC) will be determined. Evaluation of cytotoxicity will be carried out using *Artemia salina*. These biogenic AgNPs can be non-toxic and sustainable candidates for industrial waste remediation and environmental protection.

2. Materials and Methodology

2.1 Materials

Aluminum chloride ($AlCl_3$), Ammonium Molybdate [$(NH_4)_6Mo_7O_{24}$], Folin & Ciocalteu's reagent (C_6H_6O), Glacial acetic acid (CH_3COOH), Methyl Orange ($C_{14}H_{14}N_3NaO_3S$), Para-nitrophenol ($C_6H_5NO_3$), Potassium acetate ($C_2H_3O_2K$), Silver nitrate ($AgNO_3$), Sodium borohydride ($NaBH_4$), Sodium carbonate (Na_2CO_3), Sodium nitrite ($NaNO_2$), Sodium phosphate (Na_3PO_4), Sulphuric acid

(H_2SO_4).

2.2 Methodology

2.2.1 Sample Collection

The leaves of five *Curcuma* species were collected from the Arunalu plant nursery, Kurunegala, Sri Lanka (Figure 3). The sample codes are given in brackets below.

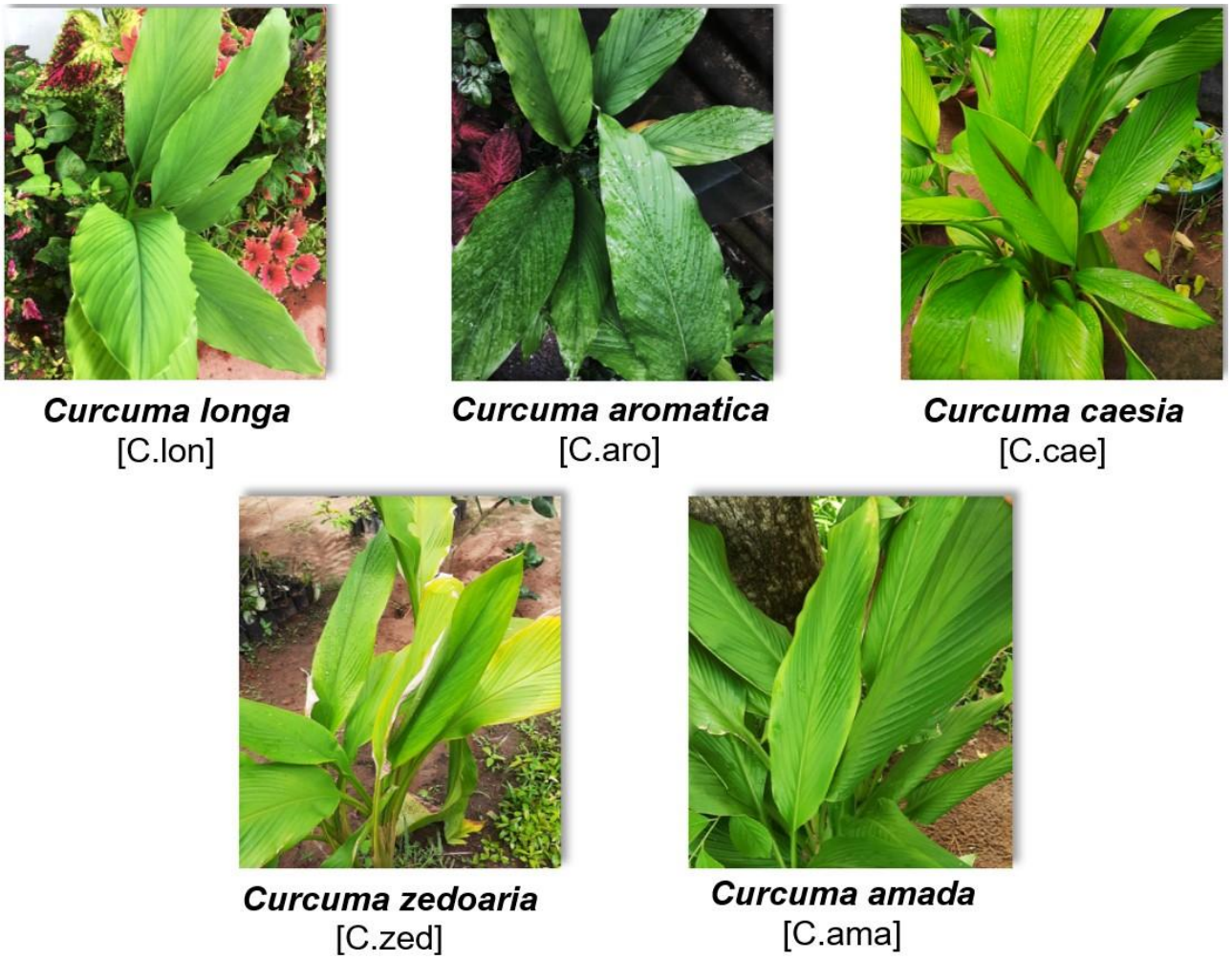

Figure 3 Leave samples selected for this study.

2.2.2 Aqueous Leaf Extraction

The collected leaves were carefully wiped with soft cloth and shade-dried for five days, followed by oven drying at 40°C for three days. Dried leaves were finely cut, and 2 g of leaves were added to 50 mL of distilled water (DW). These samples were then boiled at 100°C for 15 minutes and cooled down. Then the extracts were filtered through Whatman No. 1 filter paper. The obtained water extracts (WEs) were stored at 4°C for future use [28].

2.2.3 AgNPs Synthesis and Optimization

1 mL of WEs were added with 9 mL of 1 mM $AgNO_3$. The mixtures were subjected to optimization

at 60°C and 90°C for 15, 30, 45, and 60 mins in a dry oven and at a dark place with room temperature (RT) for 24 h. The transformation of color before and after the optimization was noted and absorbance was measured from 320-520 nm using UV-Vis spectroscopy [29].

2.2.4 Scanning Electron Microscopy (SEM)

C.zed-AgNP was centrifuged at 5000 rpm for 5 minutes and repeated until the pellet was formed, which was oven-dried at 40°C for 24 h and outsourced to SLINTEC, Sri Lanka, for the SEM analysis.

2.2.5 Antioxidant Assays

1 mL of WEs and AgNPs were diluted with 14 mL of DW (1:15) to make ×15 dilutions and stored at 4°C, which were utilized in TFC, TPC, and TAC assays.

TFC. 1.5 mL of samples were added with 0.9 mL of 3% $NaNO_2$, 0.3 mL of 10% $AlCl_3$, 0.3 mL of 1 M Potassium acetate and incubated for 30 mins at RT and performed in triplicates. The absorbance was taken at 416 nm, using the DW as the blank. The TFC of WEs and AgNPs were represented in equivalents of Quercetin standard in µg/QE/100 g [30].

TPC. 0.5 mL of samples were added with 0.75 mL of 10% Na_2CO_3, then left for 3 minutes and added with 0.95 mL of DW with 0.25 mL of 2 M Folin & Ciocalteu's phenol reagent, followed by incubation for 30 mins at RT which were carried out in triplicates. The absorbance was obtained at 750 nm, using the DW as the blank. The TPC of WEs and AgNPs were analyzed in equivalents of Gallic acid standard in mg/GAE/100 g [30].

TAC. 3 mL of Phosphomolybdenum reagent (0.6 M H_2SO_4, 28 mM Na_3PO_4, and 4 mM ammonium molybdate in 1:1:1 ratio) was prepared and added with 1 mL samples and incubated at 90°C for 90 minutes. The absorbance was attained at 695 nm, and DW was used as the blank. The TAC of WEs and AgNPs were expressed with equivalents of the Ascorbic acid standard as g/AAE/100 g [31].

2.2.6 Cytotoxicity Assay of AgNPs

Artemia salina cysts were grown in seawater for 24 h under LED light with aeration. In each well of 96 well-plate, 50 µL of 4000 ppm AgNP was added with 200 µL of sea water while 12.5 µL of AgNP was added with 237.5 µL of sea water. Each well was added with two hatched brine shrimps and left for 24 h, performed as triplicates. The control was seawater, and the percentage viability was calculated according to Equation 1 [32, 33].

$$\text{Percentage}(\%)\text{Viability} = \frac{\text{Number of alive brine shrimps}}{\text{Total number of brine shrimps}} \times 100 \quad (1)$$

2.2.7 PNP Catalysis

A PNP control is compared to the catalytic activity of AgNPs by measuring the reduction of the peak of PNP in the range of 280-540 nm, and also, the formation of the end product called PAP is confirmed with the peak at 300 nm. Firstly, using a quartz cuvette, 2 mL of 0.1 mM of PNP alone was measured for the absorbance from 280-540 nm. Then, the addition of 1 mL of 0.1 M $NaBH_4$ to

the 2 mL of 0.1 mM of PNP was evaluated, and finally, the 100 µL of 4000 ppm AgNPs with 1 mL of 0.1 M $NaBH_4$ and 2 mL of 0.1 mM of PNP. The reduction of PNP was measured every 10 minutes of interval [34].

2.2.8 Methyl-orange Photocatalysis

The photocatalytic activity of AgNP was measured by degrading the methyl-orange and tested in the presence of $NaBH_4$. These experiments were conducted under sunlight, and the absorbance was taken at room temperature. At first, 50 mL of 1 mg/100 mL Methyl-orange was added to 0.5 mL of 4000 ppm and 266.67 ppm of each AgNP, which were left under sunlight. The same procedure was performed by adding 0.5 mL of 0.2 M $NaBH_4$, and then absorbance was recorded within time intervals. The absorbance was determined from 300 to 600 nm, and the blank used was DW [35].

2.2.9 Statistical Analysis

A one-way ANOVA test was performed using Microsoft Excel, and the Pearson correlation was carried out using IBM SPSS version 29.

3. Results

3.1 AgNPs Synthesis

Temperature and time optimization produced AgNPs at RT after 24 h within 320-520 nm (Table 1).

Table 1 Optimization table.

Temperature	90°C				60°C				RT
Time	15 mins	30 mins	45 mins	60 mins	15 mins	30 mins	45 mins	60 mins	24 hours
C.lon	×	×	×	×	×	×	×	×	√
C.aro	×	×	×	×	×	×	×	×	√
C.cae	×	×	×	×	√	×	×	×	√
C.zed	×	×	×	×	√	√	√	√	√
C.ama	×	×	×	×	×	×	×	√	√

Color change from colorless to reddish-brown was observed after 24 h (Figure 4).

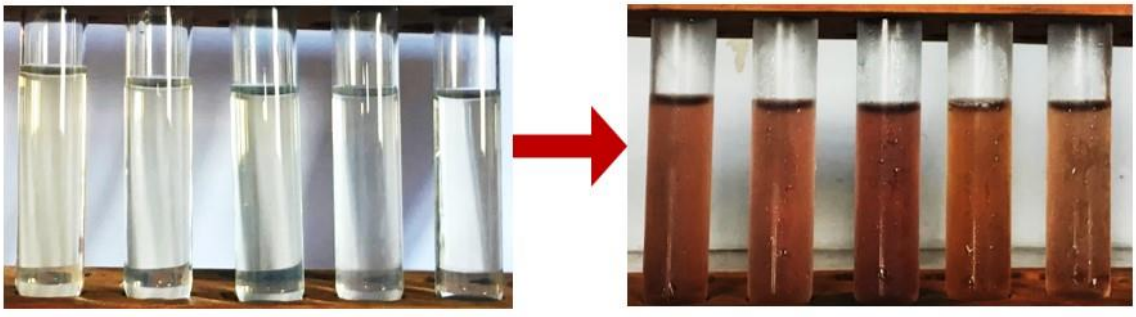

Figure 4 Before and after AgNP synthesis.

3.2 UV Characterization

AgNP peak was observed at 460 nm and 480 nm in RT for 24 h (Figure 5).

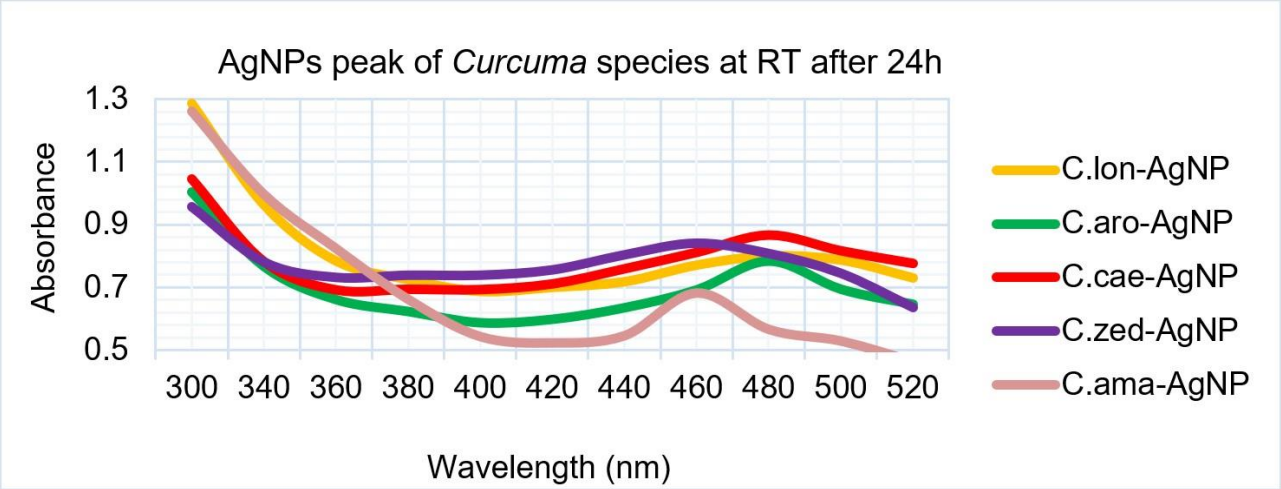

Figure 5 Peak obtained using UV spectroscopy at RT after 24 h.

3.3 SEM Characterization

Cubic AgNPs were observed with a diameter of 30-50 nm (Figure 6).

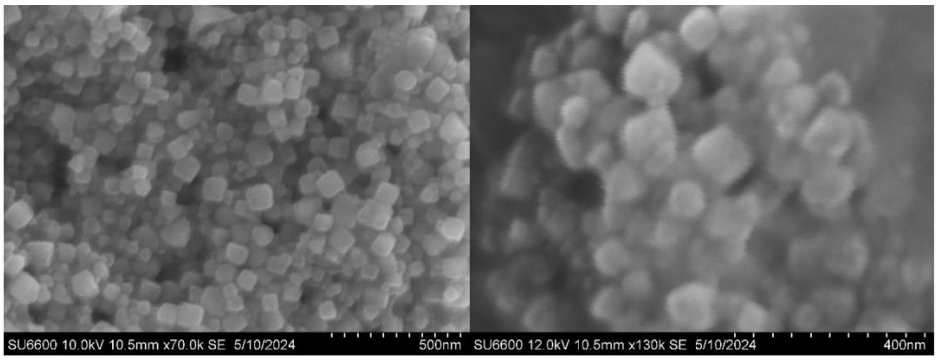

Figure 6 SEM pictures of C.zed-AgNP at 10.0 kV 10.5 mm × 70.0 k SE (left) and 12.0 kV 10.5 mm × 130 k SE (right).

3.4 Antioxidant Assays

3.4.1 TFC

The TFC of AgNPs was higher than WEs (Figure 7) and supported by the p-value of the ANOVA test (Table S1).

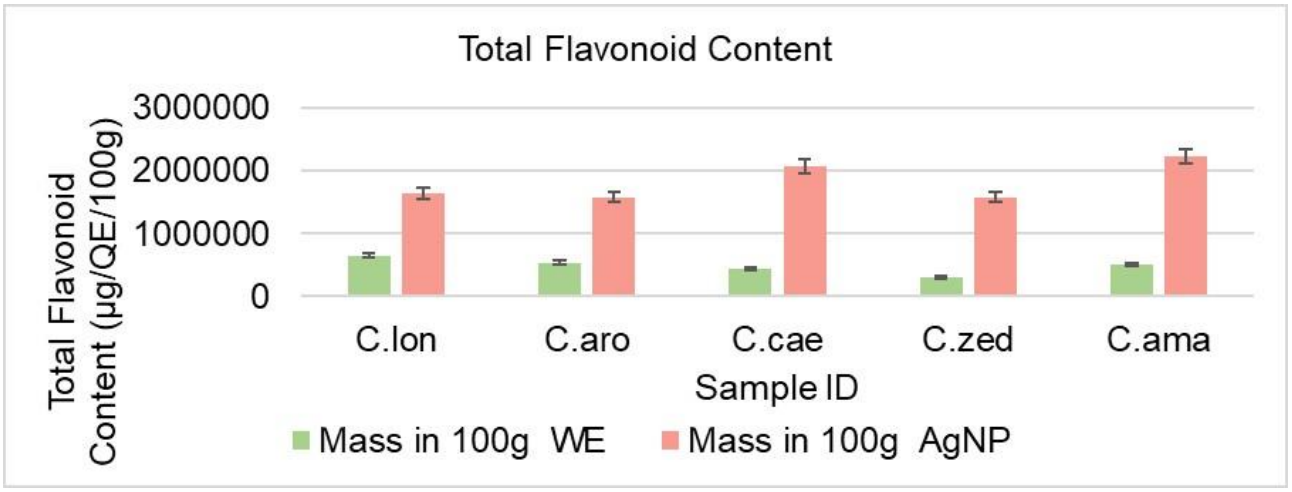

Figure 7 TFC of WEs and AgNPs as µg/QE/100 g.

3.4.2 TPC

The TPC with AgNPs was higher than the WEs (Figure 8) and confirmed by the p-value of the ANOVA test (Table S2).

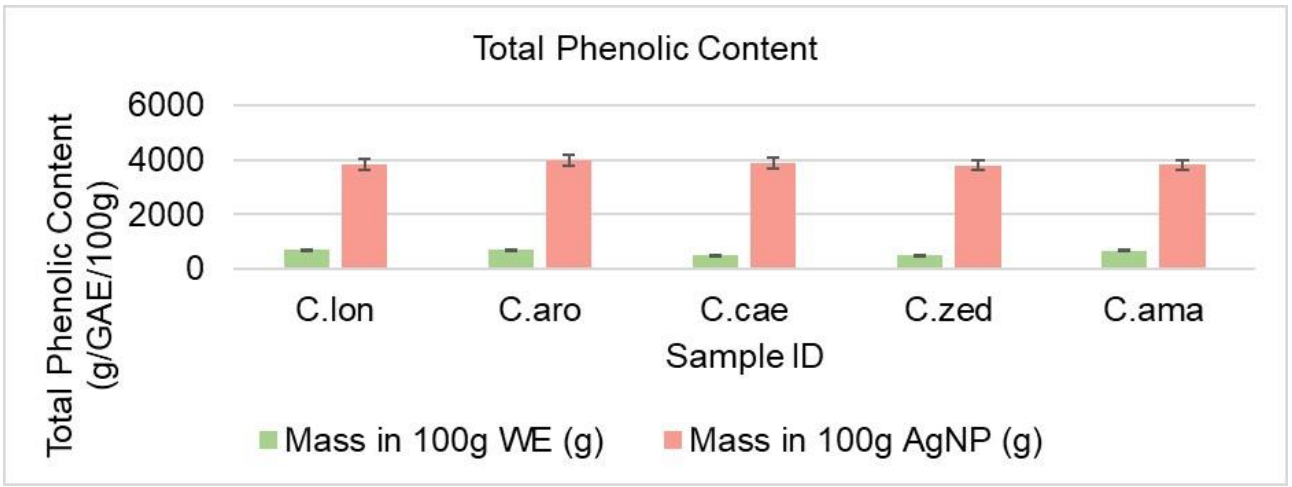

Figure 8 TPC of WEs and AgNPs as g/GAE/100 g.

3.4.3 TAC

The AgNPs demonstrated a higher TAC than WEs (Figure 9), further interpreted with the p-value obtained using the ANOVA test (Table S3).

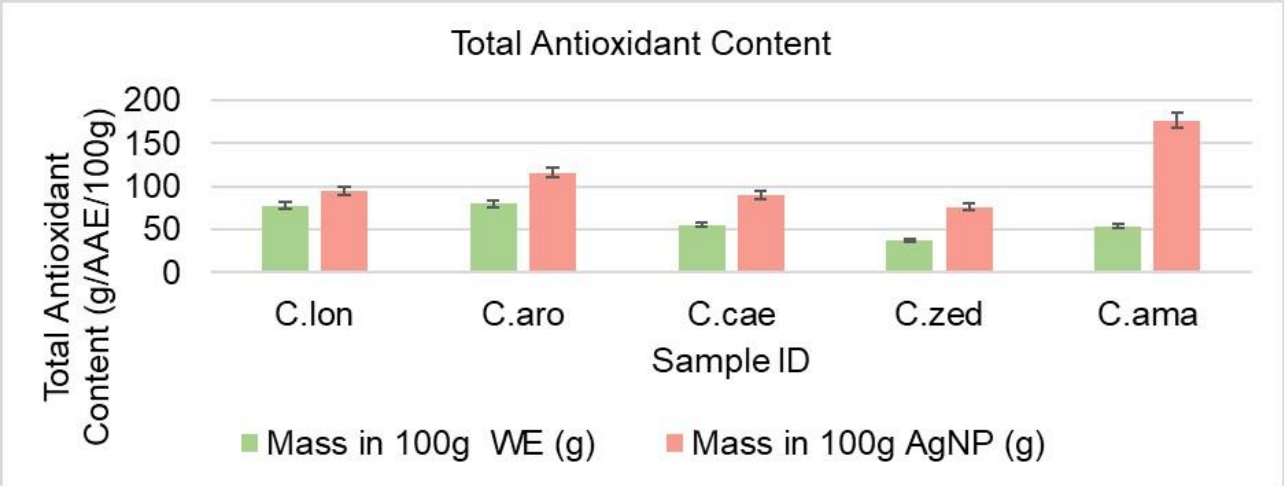

Figure 9 TAC of WEs and AgNPs as g/AAE/100 g.

3.5 Cytotoxic Assay of AgNPs

Artemia salina cysts had successfully hatched and survived after 24 h with 100% viability in all 200 ppm and 800 ppm AgNPs (Table 2).

Table 2 Viability of *Artemia salina.*

Sample	**Percentage viability**	
Control	100%	
AgNPs	**200 ppm**	**800 ppm**
C.lon-AgNP	100%	100%
C.aro-AgNP	100%	100%
C.cae-AgNP	100%	100%
C.zed-AgNP	100%	100%
C.ama-AgNP	100%	100%

3.6 PNP Catalysis Activity

All AgNPs demonstrated complete degradation of PNP and formation of PAP over 30 minutes, as confirmed by the color changes (Figure 10).

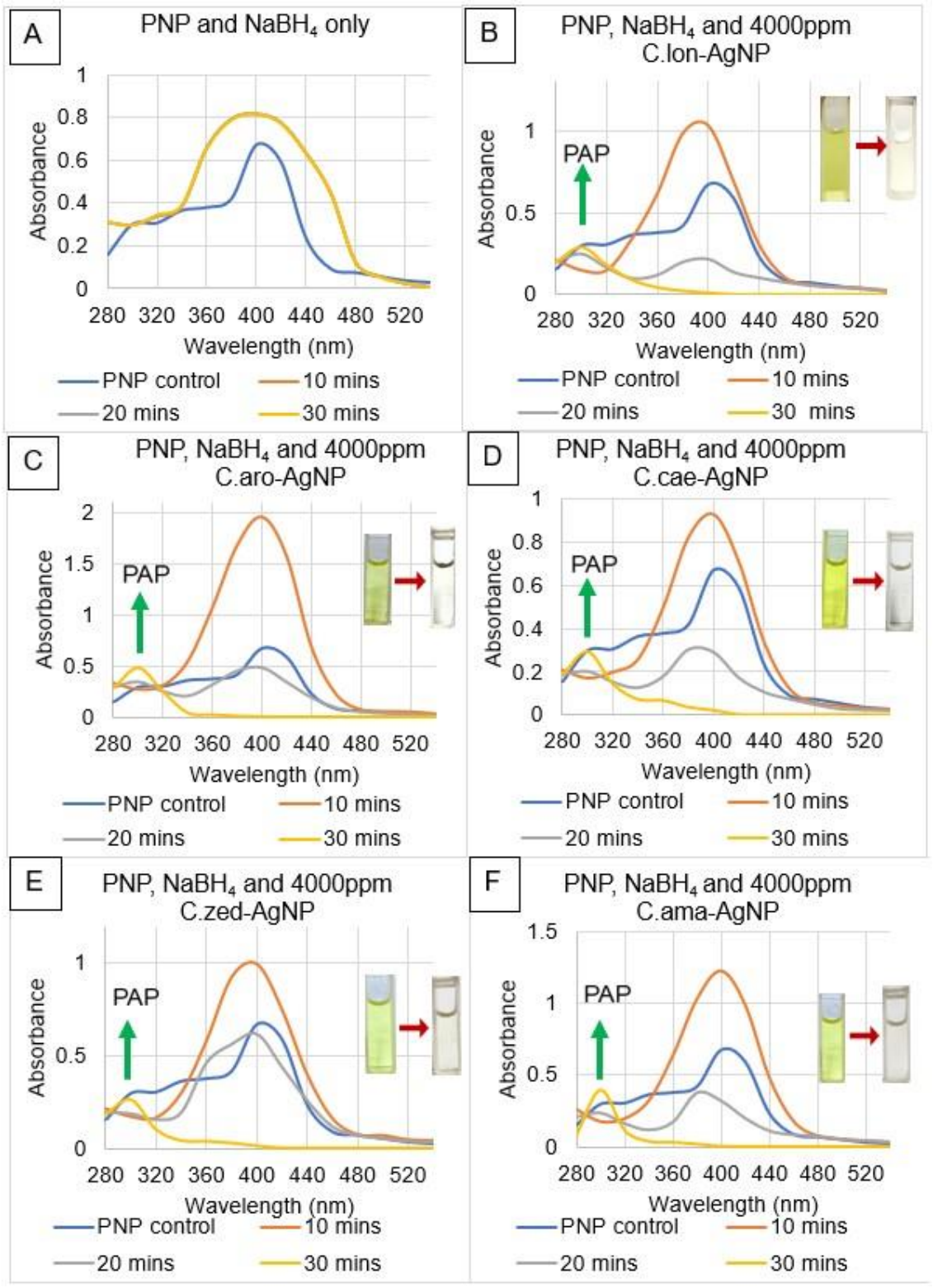

Figure 10 Results of PNP catalysis in; A) $NaBH_4$, B) C.lon-AgNP, C) C.aro-AgNP, D) C.cae-AgNP, E) C.zed-AgNP and F) C.ama-AgNP with color changes.

3.7 Photocatalysis Activity

C.lon-AgNP showed no activity under sunlight, but with $NaBH_4$, the methyl-orange degraded within 30 minutes at 4000 ppm and 266.67 ppm (Figure 11).

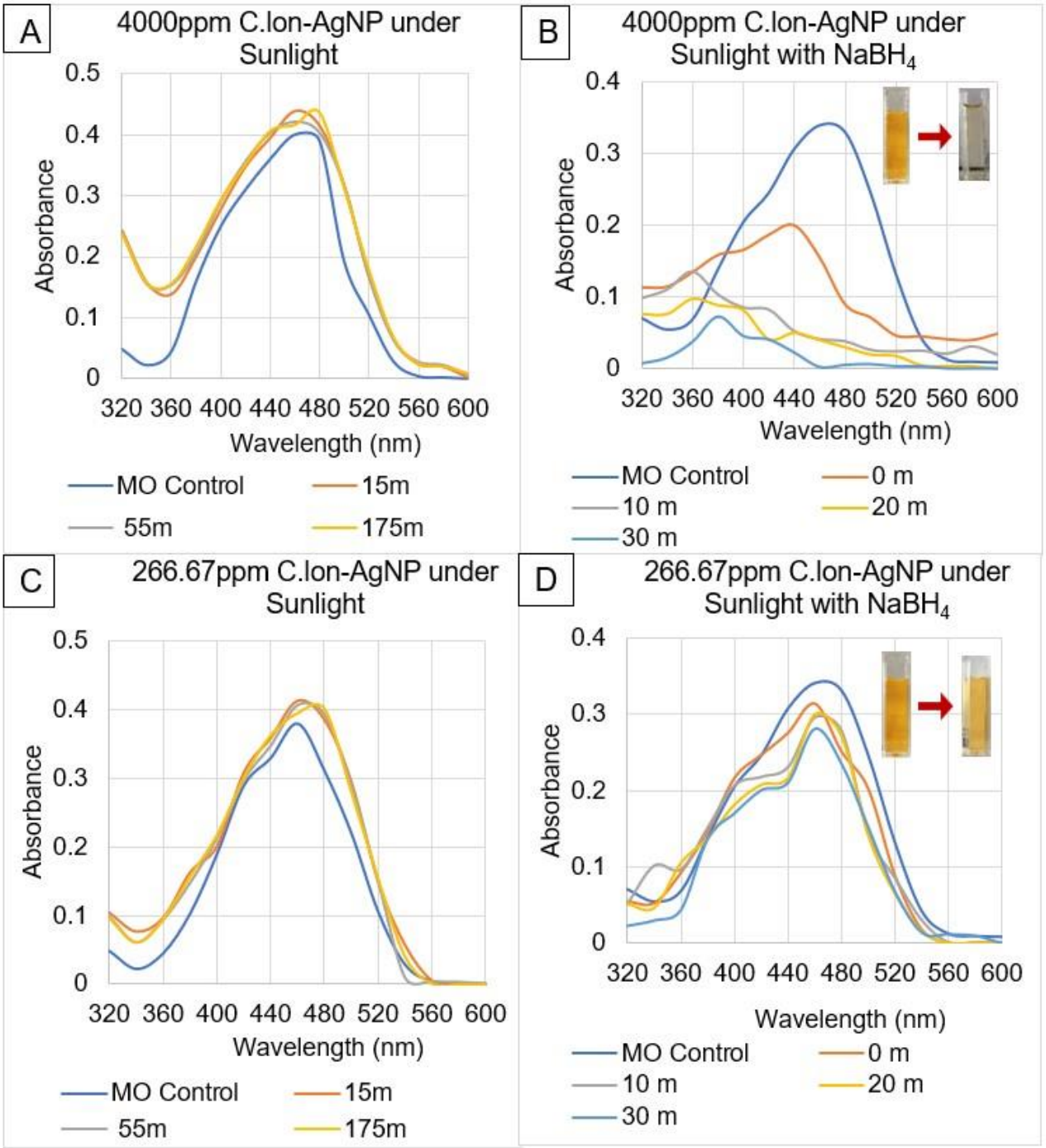

Figure 11 Methyl-orange photocatalysis by 4000 ppm C.lon-AgNP in A) sunlight, B) sunlight with $NaBH_4$, and 266.67 ppm C.lon-AgNP in C) sunlight D) sunlight with $NaBH_4$.

In sunlight, C.aro-AgNP did not catalyze, and with $NaBH_4$, the methyl-orange degraded in 30 minutes at 4000 ppm and 266.67 ppm (Figure 12).

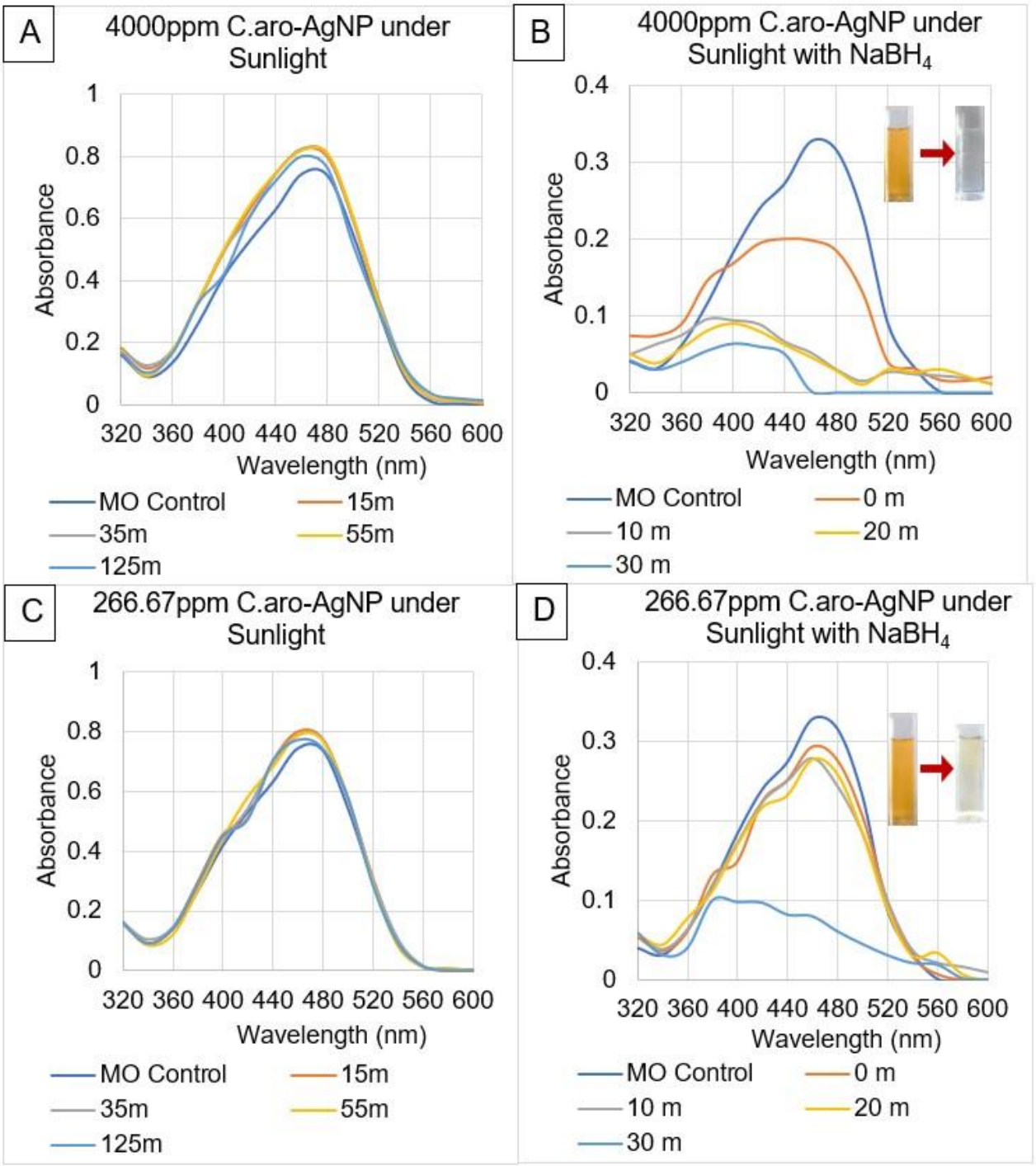

Figure 12 Methyl-orange photocatalysis by 4000 ppm C.aro-AgNP in A) sunlight, B) sunlight with $NaBH_4$, and 266.67 ppm C.aro-AgNP in C) sunlight D) sunlight with $NaBH_4$.

With sunlight, 4000 ppm C.cae-AgNP had no activity, while 266.67 ppm C.cae-AgNP showed degradation within 300 minutes. Though, with $NaBH_4$, a rapid degradation was observed in both AgNP concentrations (Figure 13).

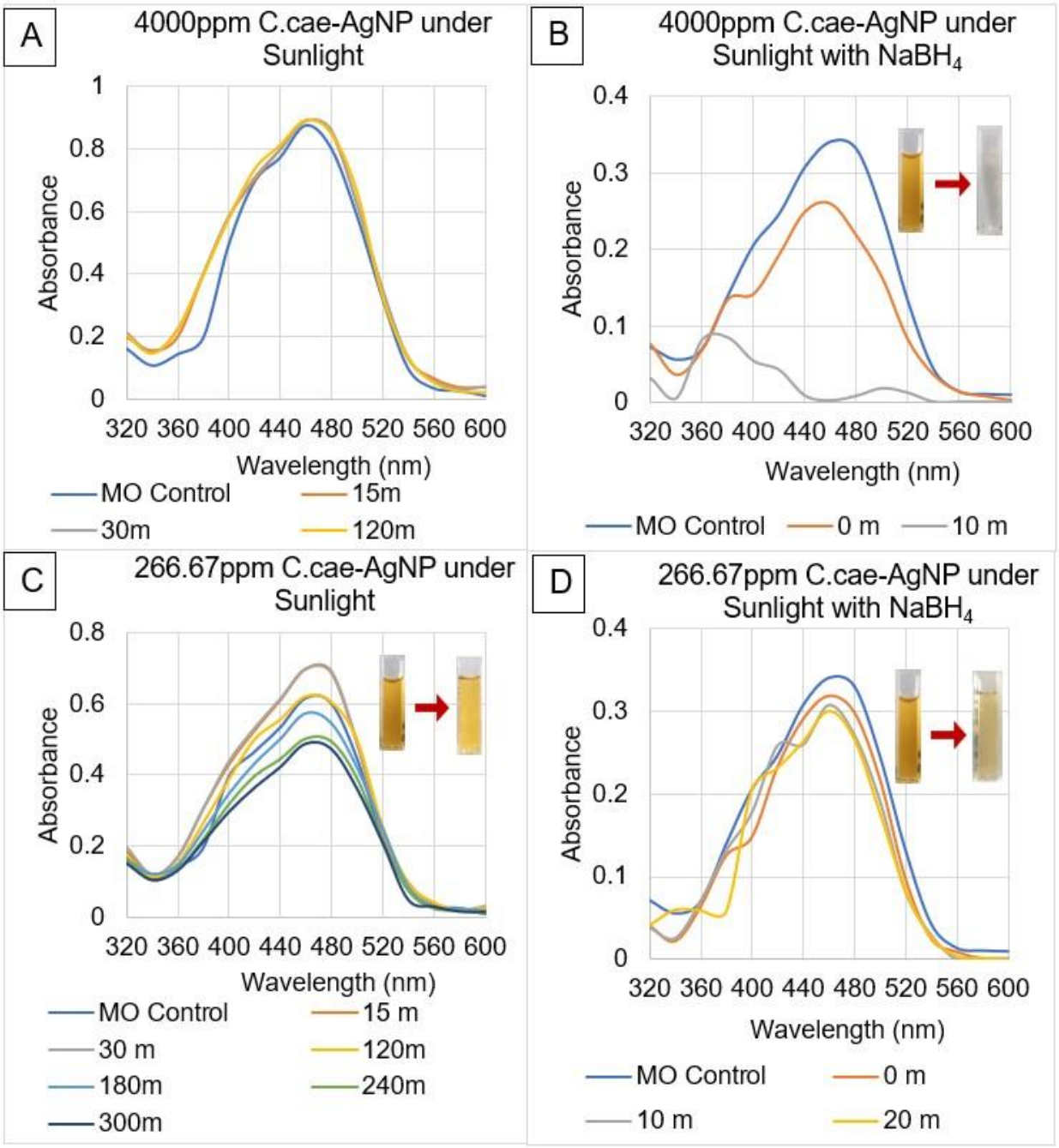

Figure 13 Methyl-orange photocatalysis by 4000 ppm C.cae-AgNP in A) sunlight B) sunlight with $NaBH_4$, and 266.67 ppm C.cae-AgNP in C) sunlight D) sunlight with $NaBH_4$.

C.zed-AgNP had a minute photocatalysis in sunlight within 300 minutes and complete degradation with $NaBH_4$ with 4000 ppm and 266.67 ppm (Figure 14).

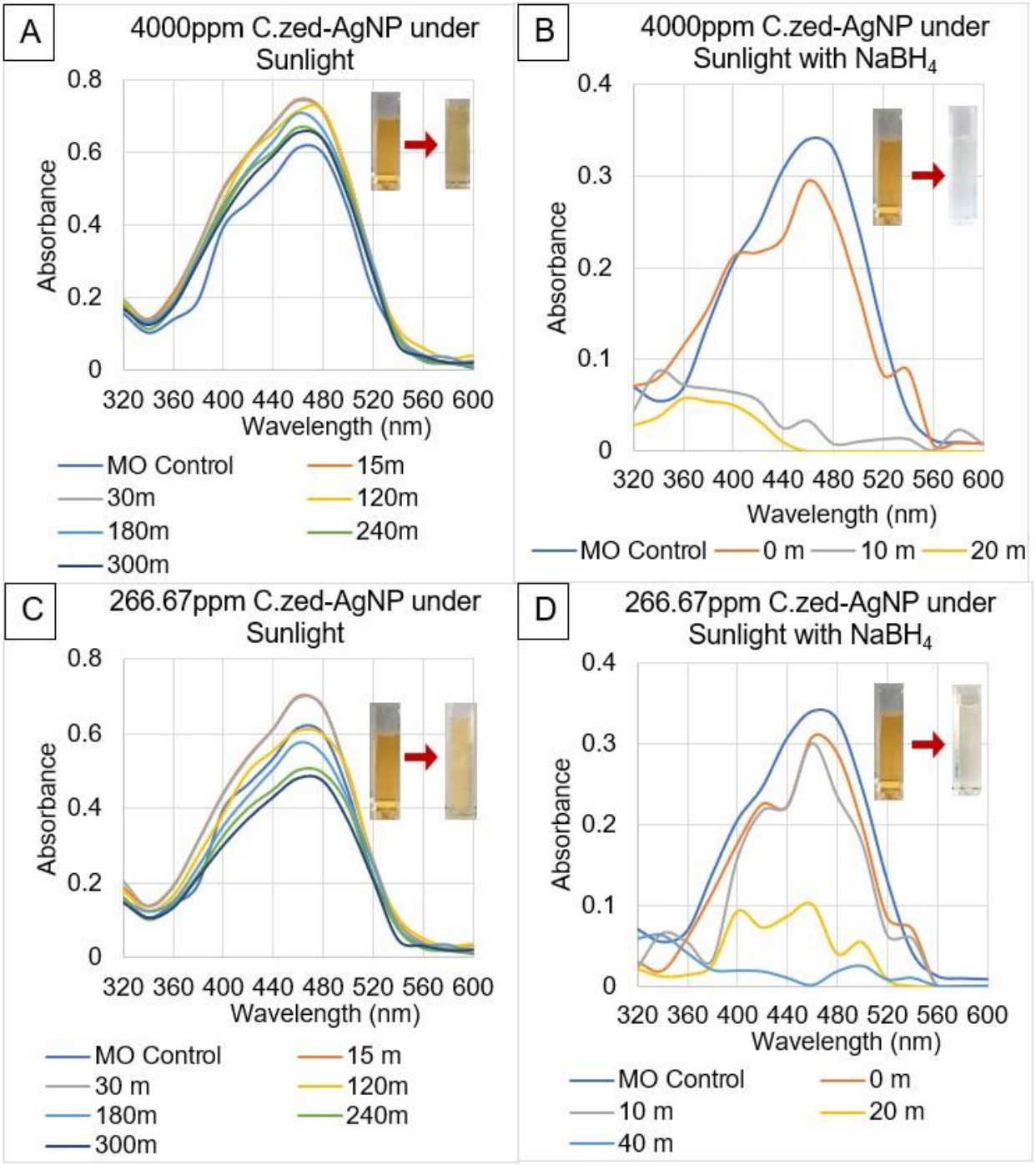

Figure 14 Methyl-orange photocatalysis by 4000 ppm C.zed-AgNP in A) sunlight B) sunlight with $NaBH_4$, and 266.67 ppm C.zed-AgNP in C) sunlight D) sunlight with $NaBH_4$.

C.ama-AgNP showed no activity under sunlight, however, photocatalyzed with $NaBH_4$ in 4000 ppm and 266.67 ppm (Figure 15).

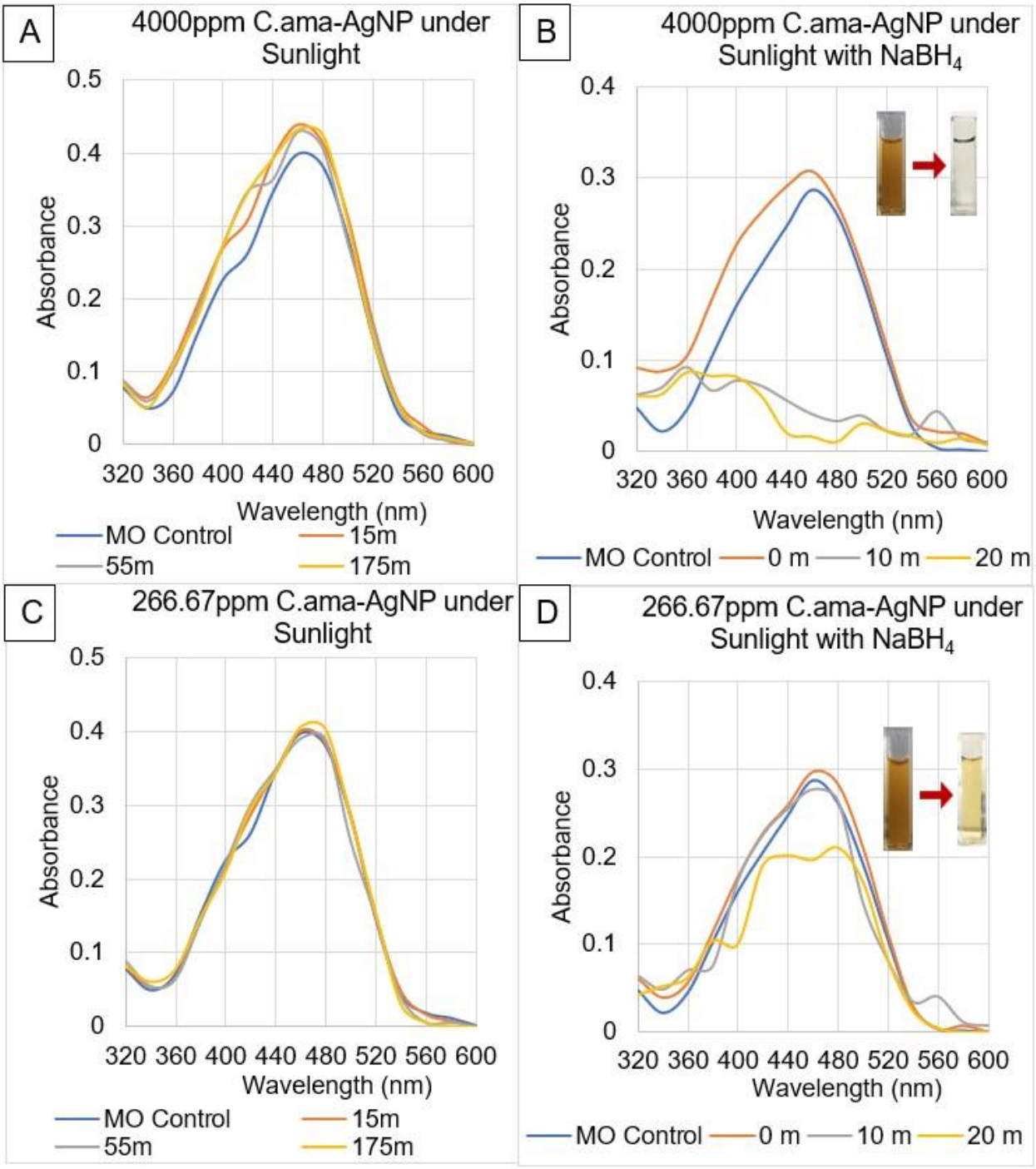

Figure 15 Methyl-orange photocatalysis by 4000 ppm C.ama-AgNP in A) sunlight, B) sunlight with $NaBH_4$, and 266.67 ppm C.ama-AgNP in C) sunlight D) sunlight with $NaBH_4$.

4. Discussion

AgNP synthesis was accomplished using five *Curcuma* species leave extracts that are eco-friendly and cost-effective, ensuring large-scale manufacturing capability. In contrast, culturing of microorganisms contributes to contamination and expenses [36]. Enhanced diffusion of biomolecules and mass transfer was achieved using water as the solvent [37]. The phytochemicals of plant extract play a significant role as the capping, reducing, and stabilizing agents of AgNP

production, which consist of the activation stage where the Ag^+ is reduced to Ag^0 with a nucleus, and in the growth stage, small AgNPs spontaneously coalescent to large AgNPs through Ostwald ripening determining the shape and size of the AgNPs [38]. The AgNPs were initially confirmed with the color transformation to reddish-brown, as demonstrated in Figure 4, which is due to the SPR property that causes the resonance effect of conduction electrons at the surface of AgNPs and the change of state from Ag^+ to Ag^0 [39]. UV characterization of AgNPs had formed peaks (Figure 5) with respect to SPR electron oscillation at 480nm for C.lon-AgNP, C.aro-AgNP, C.cae-AgNP and at 460 nm for C.zed-AgNP and C.ama-AgNP which highlights that the AgNPs formed are polydisperse as well as smaller due to longer wavelength [40]. Concurrently, research studies of [41] on *Curcuma* species also produced a peak around 475 nm. Furthermore, since the AgNPs were formed at RT for 24 h, it could suggest a fast growth of AgNPs without the need for a higher temperature to support the reaction. At 90°C and 60°C during the optimization (Table 1) the peaks were found at a higher wavelength, which was not within 420-480 nm, depicting an aggregated AgNP growth [42]. These peaks were confirmed with SEM characterization, which revealed cubic AgNPs with varying diameters from 30-50 nm (Figure 6).

To analyze the conductivity of AgNPs, it is essential to determine the band gap energy, which refers to the minimum energy required by the electrons to jump from valence to the conduction band. Insulators require >4 eV of energy while semiconductors need <3 eV to transfer into the excitation state [43], whereby all the synthesized AgNPs were semiconductors according to the Equation 2 [44] with respect to the peaks produced at 460 nm and 480 nm (Table 3).

$$\mathrm{E(J)} = \frac{\hbar(\text{Planks contant}, 6.626 \times 10^{-34}) \times \mathrm{C}(\text{Speed of light}, 3 \times 10^{8})}{\lambda(\text{Wavelength of AgNP} \times 10^{-9})} \quad (2)$$

Table 3 The evaluated band gap energy of AgNPs.

Sample	Bandgap Energy (J)	Bandgap Energy (eV)	Classification
C.lon-AgNP	4.14125×10^{-19}	2.58	Semiconductor
C.aro-AgNP	4.14125×10^{-19}	2.58	
C.cae-AgNP	4.14125×10^{-19}	2.58	
C.zed-AgNP	4.3213×10^{-19}	2.70	
C.ama-AgNP	4.3213×10^{-19}	2.70	

Flavonoids and phenols hold an aromatic ring with at least one hydroxyl-group, which can donate electrons, providing an antioxidant action [45]. The TFC determination using $AlCl_3$ colorimetric assay forms acid-stable complexes when $AlCl_3$ binds to flavonoids through C4 keto-group with C3/C5 hydroxyl-group and acid-labile complexes with ortho-dihydroxyl-groups of A/B-ring with maximum absorbance at 416 nm. The TFC results in Figure 7 demonstrated that all AgNPs have higher levels of TFC than WEs in the order of C.ama-AgNP = C.cae-AgNP > C.lon-AgNP = C.ama-AgNP which correlated with the research of [46]. In addition, the ANOVA test between WEs and AgNPs (Table S1) also provided a lower p-value of 1.97174×10^{-5} (<0.05) and a smaller F-crit than F-value approving a significant difference.

The TPC was assessed using a Folin-Ciocalteu colorimetric assay. The results of TPC (Figure 8) proved that all AgNPs were high in phenolic content over WEs with the significant difference claimed

through the ANOVA test (Table S2) where the p-value was 1.38×10^{-11} (<0.05), and F-crit was lower than F-value. Moreover, research [46] also reported comparable findings.

The TAC was determined through the phosphomolybdenum assay. The AgNPs were significantly higher in TAC than the WEs in the order of C.ama-AgNP > C.aro-AgNP > C.lon-AgNP > C.cae-AgNP > C.zed-AgNP (Figure 9). A study of [17] has reported similar findings. The ANOVA test revealed a significant difference as the P-value was 0.032536 (<0.05) and the F-crit was also lesser than F value (Table S3).

Furthermore, correlation statistics were performed to determine the relation among the antioxidant assays, and a strong correlation (>0.5) was seen with TFC and TPC. In contrast, a moderate positive correlation was observed between TAC, TFC and TPC, as in Figure 16. The relationship between TFC and TPC was highly linkable, resulting in an overall antioxidant activity. A study of [47] had also produced a strong TFC-TPC correlation.

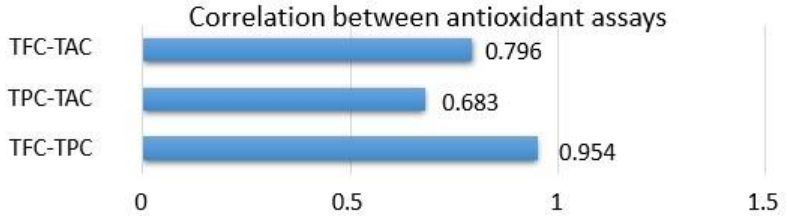

Figure 16 Pearson correlation coefficient.

Cytotoxicity assay revealed that all 200 ppm and 800 ppm AgNPs had 100% viability of brine shrimps, according to Table 2. Moreover, the experimentation of [48] also proved that AgNPs are non-toxic with the concentration-dependent study.

The catalytic and photocatalytic activity was determined using the pseudo-first-order kinetics according to Equation 3 [49] since it is a rate-determining step.

$$\ln\left(\frac{\boldsymbol{C_t}(\text{Peak concentration})}{\boldsymbol{C_0}(\text{Initial concentration})}\right) = \boldsymbol{k}(\text{Rate constant}) \times \boldsymbol{t}(\text{Time at peak concentration}) \qquad (3)$$

AgNPs catalyze and degrade PNP with the presence of $NaBH_4$ by lowering the activation energy and transferring six electrons per PNP molecule (Figure 17).

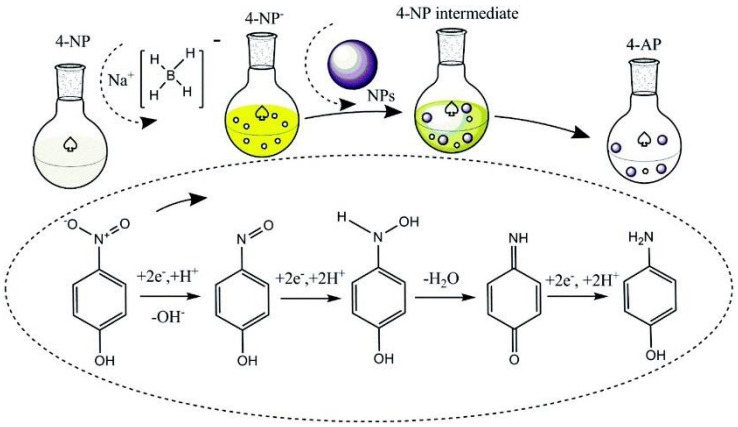

Figure 17 Catalytic degradation of p-nitrophenol (PNP) to p-aminophenol (PAP) [50].

According to the research of [51], the Langmuir−Hinshelwood (LH) model suggests that AgNPs react with borohydride ions (BH_4^-) to form silver hydride. At the same time, PNP simultaneously adsorbs on the AgNP surface, reducing the adsorbed PNP to PAP, which will be desorbed again, and the AgNPs will catalyze another PNP molecule. The PNP degradation was observed with the reduction of PNP peak at 400 nm by all the AgNPs in Figure 10 within 30 minutes, while elevation of PAP can be seen at 300 nm. The PNP degradation can be supported by the color change from fluorescent yellow to colorless. The PNP control also produced a modest peak at 300 nm, which might have occurred due to the presence of hydroperoxyl radicals formed by water [52]. Furthermore, the rate constant value of PNP degradation kinetics was significantly high with C.aro-AgNP and C.ama-AgNP followed by other AgNPs (Figure S1 and Table 4), whereby research of [49] emphasizes that the tremendous catalytic activity is due to smaller AgNPs which facilitate more electron transfer from the AgNP surface. A study [53] also demonstrated a similar and rapid PNP degradation with AgNPs.

Table 4 Rate constant values of PNP catalysis by AgNPs.

PNP degradation rate-constant value	
Sample	**Rate constant value (k)**
C.lon-AgNP	0.0615
C.aro-AgNP	0.0908
C.cae-AgNP	0.0509
C.zed-AgNP	0.0557
C.ama-AgNP	0.0817

Photocatalysis was focused on degrading methyl-orange using AgNPs. The UV rays of sunlight excite electrons from valence to the conduction band in AgNPs, which drives the formation of ROS from the available water and oxygen around the AgNPs. Consequently, ROS attacks the azo bond (N=N), resulting in the degradation of methyl- orange while the addition of $NaBH_4$ facilitates more electrons on the AgNP surface as a nucleophile catalyst [54]. Under sunlight, none of the 4000 ppm or 266.67 ppm AgNPs degraded significantly; however, favorably, under sunlight with $NaBH_4$, all 4000 ppm and 266.67 ppm AgNPs rapidly degraded the methyl-orange (Figures 11 to 15), with corresponding kinetics of R^2-value (coefficient of determination) closer to 1 (Figure S2). Critically, C.zed-AgNP was photocatalyzed under sunlight with $NaBH_4$, which had the highest activity and kinetics of other AgNPs (Table 5). A study [55] also demonstrated methyl-orange degradation by AgNPs within 11 minutes.

Table 5 Rate constant values of Methyl-orange photocatalysis by AgNPs.

Methyl-orange degradation rate-constant value		
Sample	**Sunlight with $NaBH_4$**	
	4000 ppm	266.67 ppm
C.lon-AgNP	0.0671	0.0025
C.aro-AgNP	0.067	0.0184
C.cae-AgNP	0.223	0.0027
C.zed-AgNP	0.1013	0.0661
C.ama-AgNP	0.0627	0.0083

In the future, dinitrophenol can be tested for catalytic activity since it is used in industries and can harm the marine-organisms. Also, formaldehyde production from methanol can be catalyzed with AgNPs, while industrial demands such as ketones and aldehydes can be provided with alcohol dehydrogenation. Photocatalysis of azo-dyes like malachite-green, methyl-blue, and methyl-red can be examined since many of the azo-dyes contribute to toxicity.

5. Conclusions

This study successfully synthesized the AgNPs using five *Curcuma* species' leaves at RT for 24 h, which were defined with peaks at 460 nm and 480 nm in UV-Vis spectrometry and were disclosed as semi-conductors and proved with SEM analysis, which showed 30-50 nm sized cubic nanoparticles. All AgNPs showed excellent antioxidant activity with higher TFC, TPC, and TAC than the WEs. 200 ppm and 800 ppm AgNPs provided 100% viability of *Artemia salina,* ensuring non-toxicity. PNP catalysis of all AgNPs was completed within 30 minutes, and photocatalysis of methyl-orange by all 4000 ppm and 266.67 ppm AgNPs was achieved with $NaBH_4$ while C.zed-AgNP showed greater photocatalysis with the addition of $NaBH_4$.

Acknowledgments

The authors are acknowledging the support provided by Northumbria University, UK in PNP catalysis.

Author Contributions

Dean and senior supervisor Dr. Mathi Kandiah carried out the planning and design of the research and analyzed with revision of manuscript. Experiments were executed and recorded by Dharsha Bhaskaran. Ominda Perera has overlooked the experiment work.

Funding

Authors thank BMS for funding.

Competing Interests

The authors have declared that no competing interests exist.

Data Availability Statement

Further data relevant to this research can be requested from the authors at mathi@bms.ac.lk.

Additional Materials

The following additional materials are uploaded at the page of this paper.

1. Table S1: ANOVA test for TFC.
2. Table S2: ANOVA test for TPC.
3. Table S3: ANOVA test for TAC.

4. Table S4: Determination of rate constant with C.lon AgNP in Sunlight and $NaBH_4$.
5. Table S5: Determination of rate constant with C.aro-AgNP in Sunlight and $NaBH_4$.
6. Table S6: Determination of rate constant with C.cae-AgNPs in Sunlight.
7. Table S7: Determination of rate constant with C.cae-AgNPs in Sunlight and $NaBH_4$.
8. Table S8: Determination of rate constant with C.zed-AgNPs in Sunlight.
9. Table S9: Determination of rate constant with C.zed-AgNPs in Sunlight and $NaBH_4$.
10. Table S10: Determination of rate constant with C.ama-AgNPs in Sunlight and $NaBH_4$.
11. Figure S1: Rate constant graphs for 4000 ppm AgNPs in PNP degradation.
12. Figure S2: Rate constant graph for methyl-orange photocatalytic activity in sunlight and $NaBH_4$ with 4000 ppm AgNPs (left), and 266.67 ppm AgNPs (right).

References

1. Fadilah NI, Isa IL, Zaman WS, Tabata Y, Fauzi MB. The effect of nanoparticle-incorporated natural-based biomaterials towards cells on activated pathways: A systematic review. Polymers. 2022; 14: 476.
2. Islam MA, Jacob MV, Antunes E. A critical review on silver nanoparticles: From synthesis and applications to its mitigation through low-cost adsorption by biochar. J Environ Manag. 2021; 281: 111918.
3. Kumar D, Kumar P, Singh H, Agrawal V. Biocontrol of mosquito vectors through herbal-derived silver nanoparticles: Prospects and challenges. Environ Sci Pollut Res. 2020; 27: 25987-26024.
4. Aguilar ZP. Nanotoxicology and remediation. In: Nanomaterials for medical applications. Amsterdam, Netherlands: Elsevier; 2013. pp. 361-408.
5. Ghotekar S, Pansambal S, Bilal M, Pingale SS, Oza R. Environmentally friendly synthesis of Cr_2O_3 nanoparticles: Characterization, applications and future perspective – A review. Case Stud Chem Environ Eng. 2021; 3: 100089.
6. Nguyen DH, Vo TN, Le NT, Thi DP, Thi TT. Evaluation of saponin-rich/poor leaf extract-mediated silver nanoparticles and their antifungal capacity. Green Process Synth. 2020; 9: 429-439.
7. Gudikandula K, Charya S. Synthesis of silver nanoparticles by chemical and biological methods and their antimicrobial properties. J Exp Nanosci. 2016; 11: 714-721.
8. Moomin A, Russell WR, Knott RM, Scobbie L, Mensah KB, Adu-Gyamfi PK, et al. Season, storage and extraction method impact on the phytochemical profile of *Terminalia ivorensis*. BMC Plant Biol. 2023; 23: 162.
9. Patil S, Chandrasekaran R. Biogenic nanoparticles: A comprehensive perspective in synthesis, characterization, application and its challenges. J Genet Eng Biotechnol. 2020; 18: 67.
10. Peng Y, Ao M, Dong B, Jiang Y, Yu L, Chen Z, et al. Anti-inflammatory effects of curcumin in the inflammatory diseases: Status, limitations and countermeasures. Drug Des Dev Ther. 2021; 15: 4503-4525.
11. Rahaman MM, Rakib A, Mitra S, Tareq AM, Emran TB, Shahid-Ud-Daula AF, et al. The genus *curcuma* and inflammation: Overview of the pharmacological perspectives. Plants. 2020; 10: 63.
12. Rodríguez FF, Graciano-Verdugo AZ, Moreno-Vásquez MJ, Lagarda-Díaz I, Barreras-Urbina CG, Armenta-Villegas L, et al. Trends in sustainable green synthesis of silver nanoparticles using agri-food waste extracts and their applications in health. J Nanomater. 2022; 2022: 8874003.
13. Sengul AB, Asmatulu E. Toxicity of metal and metal oxide nanoparticles: A review. Environ Chem

Lett. 2020; 18: 1659-1683.
14. Rajabi S, Ramazani A, Hamidi M, Naji T. *Artemia salina* as a model organism in toxicity assessment of nanoparticles. DARU J Pharm Sci. 2015; 23: 20.
15. Zehiroglu C, Ozturk SS. The importance of antioxidants and place in today's scientific and technological studies. J Food Sci Technol. 2019; 56: 4757-4774.
16. Rajendran P, Nandakumar N, Rengarajan T, Palaniswami R, Gnanadhas EN, Lakshminarasaiah U, et al. Antioxidants and human diseases. Clin Chim Acta. 2014; 436: 332-347.
17. Sivakumar T. In vitro antioxidant, total phenolic, total flavonoid content and biosynthesis of silver nanoparticles using Cassia auriculata leaves extracts. Int J Botany Stud. 2021; 6: 476-480.
18. Akintola A, Kehinde B, Ayoola P, Adewoyin A, Adedosu O, Ajayi J, et al. Antioxidant properties of silver nanoparticles biosynthesized from methanolic leaf extract of Blighia Sapida. IOP Conf Ser Mater Sci Eng. 2020; 805: 012004.
19. Kanimozhi S, Kanthimathi M. Green nanoparticles for industrially important reactions. In: Nanoparticles in green organic synthesis. Amsterdam, Netherlands: Elsevier; 2023. pp. 453-465.
20. Xu J, Wang B, Zhang W, Zhang FJ, Deng YD, Wang Y, et al. Biodegradation of p-nitrophenol by engineered strain. AMB Express. 2021; 11: 124.
21. Kahraman HT. Synthesis of silver nanoparticles using *Alchemilla vulgaris* and *Helichrysum arenarium* for methylene blue and 4-nitrophenol degradation and antibacterial applications. Biomass Convers Biorefinery. 2024; 14: 13479-13490.
22. Shimoga G, Palem RR, Lee SH, Kim SY. Catalytic degradability of p-nitrophenol using ecofriendly silver nanoparticles. Metals. 2020; 10: 1661.
23. Barciela P, Perez VA, Prieto MA. Azo dyes in the food industry: Features, classification, toxicity, alternatives, and regulation. Food Chem Toxicol. 2023; 178: 113935.
24. Chung KT. Azo dyes and human health: A review. J Environ Sci Health C. 2016; 34: 233-261.
25. Selvaraj V, Swarna KT, Mansiya C, Alagar M. An over review on recently developed techniques, mechanisms and intermediate involved in the advanced azo dye degradation for industrial applications. J Mol Struct. 2021; 1224: 129195.
26. Pingale SS, Rupanar SV, Chaskar M. Plant-mediated biosynthesis of silver nanoparticles from Gymnema sylvestre and their use in phtodegradation of Methyl orange dye. J Water Environ Nanotechnol. 2018; 3: 106-115.
27. Ganapathy Selvam G, Sivakumar K. Phycosynthesis of silver nanoparticles and photocatalytic degradation of methyl orange dye using silver (Ag) nanoparticles synthesized from *Hypnea musciformis* (Wulfen) JV Lamouroux. Appl Nanosci. 2015; 5: 617-622.
28. Beegum S, David S. Short communication investigation of antimicrobial activity of plant-mediated green synthesis of silver nanoparticles. Int J Nanosci Nanotechnol. 2022; 18: 265-274.
29. Bandaranayake SL, Perera O, Kandiah M. One pot biological synthesis of silver nanoparticles using dracaena plant leaf varieties and assessing their antioxidant, photocatalytic, antimicrobial properties, and melamine adulteration. BMS J Appl Learn. 2023; 1: 90-108.
30. Kim S, Ko SC, Kim YS, Ha SK, Park HY, Park Y, et al. Determination of *Curcuma longa* L. (Turmeric) leaf extraction conditions using response surface methodology to optimize extraction yield and antioxidant content. J Food Qual. 2019; 2019: 7575206.
31. Barbosa GB, Minguillan J. Antioxidant activity and total phenolic content of fresh and cured rhizomes of Curcuma longa and Etlingera Philippinensis. Int Food Res J. 2021; 28: 839-847.
32. Arulvasu C, Jennifer SM, Prabhu D, Chandhirasekar D. Toxicity effect of silver nanoparticles in

brine shrimp *Artemia*. Sci World J. 2014; 2014: 256919.
33. Kamiloglu S, Sari G, Ozdal T, Capanoglu E. Guidelines for cell viability assays. Food Front. 2020; 1: 332-349.
34. Kästner C, Thünemann AF. Catalytic reduction of 4-nitrophenol using silver nanoparticles with adjustable activity. Langmuir. 2016; 32: 7383-7391.
35. Kandiah M, Chandrasekaran KN. Green synthesis of silver nanoparticles using *Catharanthus Roseus* flower extracts and the determination of their antioxidant, antimicrobial, and photocatalytic activity. J Nanotechnol. 2021; 2021:5512786.
36. Tariq M, Mohammad KN, Ahmed B, Siddiqui MA, Lee J. Biological synthesis of silver nanoparticles and prospects in plant disease management. Molecules. 2022; 27: 4754.
37. Plaskova A, Mlcek J. New insights of the application of water or ethanol-water plant extract rich in active compounds in food. Front Nutr. 2023; 10: 1118761.
38. Kahsay MH, Ramadevi D, Kumar YP, Mohan BS, Tadesse A, Battu G, et al. Synthesis of silver nanoparticles using aqueous extract of Dolichos lablab for reduction of 4-Nitrophenol, antimicrobial and anticancer activities. OpenNano. 2018; 3: 28-37.
39. Liaqat N, Jahan N, Khalil UR, Anwar T, Qureshi H. Green synthesized silver nanoparticles: Optimization, characterization, antimicrobial activity, and cytotoxicity study by hemolysis assay. Front Chem. 2022; 10: 952006.
40. Miranda A, Akpobolokemi T, Chung E, Ren G, Abraham BT. pH Alteration in plant-mediated green synthesis and its resultant impact on antimicrobial properties of silver nanoparticles (AgNPs). Antibiotics. 2022; 11: 1592.
41. Shameli K, Ahmad MB, Zamanian A, Sangpour P, Shabanzadeh P, Abdollahi Y, et al. Green biosynthesis of silver nanoparticles using Curcuma longa tuber powder. Int J Nanomed. 2012; 7: 5603-5610.
42. Piñero S, Camero S, Blanco S. Silver nanoparticles: Influence of the temperature synthesis on the particles' morphology. J Phys Conf Ser. 2017; 786: 012020.
43. Sundeep D, Vijaya Kumar T, Rao PS, Ravikumar RV, Gopala Krishna A. Green synthesis and characterization of Ag nanoparticles from *Mangifera indica* leaves for dental restoration and antibacterial applications. Prog Biomater. 2017; 6: 57-66.
44. Adur AJ, Nandini N, Mayachar KS, Ramya R, Srinatha N. Bio-synthesis and antimicrobial activity of silver nanoparticles using anaerobically digested parthenium slurry. J Photochem Photobiol B Biol. 2018; 183: 30-34.
45. Aryal S, Baniya MK, Danekhu K, Kunwar P, Gurung R, Koirala N. Total phenolic content, flavonoid content and antioxidant potential of wild vegetables from western Nepal. Plants. 2019; 8: 96.
46. Zahra G, Parichehr H, Hanie S, Walker TR. Eco-friendly green synthesis and characterization of silver nanoparticles by *Scutellaria multicaulis* leaf extract and its biological activities. Pharmaceuticals. 2023; 16: 992.
47. Kandiah M, Sathishkumar A. Biogenic synthesis of silver nanoparticles using the extract of environmentally benign plant material, basil (*Ocimum Basilicum*) and determination of their antioxidant, antibacterial and photocatalytic activities. Int J Nanomater Mol Nanotechnol. 2021; 3: 122.
48. Singh R, Sagar NA, Kumar N. Bio-inspired green fabrication of silver nanoparticles (AgNPs) using aqueous leaves extract of *Ipomoea carnea* Jacq. To tackle multiple drug resistance MTCC bacterial strains. Eur J Med Chem Rep. 2022; 6: 100066.

49. Sudhakar P, Soni H. Catalytic reduction of Nitrophenols using silver nanoparticles-supported activated carbon derived from agro-waste. J Environ Chem Eng. 2018; 6: 28-36.
50. Mejía YR, Reddy Bogireddy NK. Reduction of 4-nitrophenol using green-fabricated metal nanoparticles. RSC Adv. 2022; 12: 18661-18675.
51. Baruah B, Gabriel GJ, Akbashev MJ, Booher MR. Facile synthesis of silver nanoparticles stabilized by cationic polynorbornenes and their catalytic activity in 4-nitrophenol reduction. Langmuir. 2013; 29: 4225-4234.
52. Zhao S, Ma H, Wang M, Cao C, Yao S. Study on the role of hydroperoxyl radical in degradation of p-nitrophenol attacked by hydroxyl radical using photolytical technique. J Photochem Photobiol A. 2013; 259: 17-24.
53. Chandhru M, Gunasekaran P, Maruthupandi M, Meenakshi R, Sundar M, Kalanthoden AN, et al. Bio-fabricated silver nanocatalyst for photocatalytic degradation and organic transformation of toxic pollutants. Next Mater. 2023; 1: 100023.
54. Piella J, Bastús NG, Casals E, Puntes V. Characterizing nanoparticles reactivity: Structure-photocatalytic activity relationship. J Phys Conf Ser. 2013; 429: 012040.
55. Hashemi Z, Mizwari ZM, Aghdam MS, Derazkola MS, Ebrahimzadeh MA. Sustainable green synthesis of silver nanoparticles using Sambucus ebulus phenolic extract (AgNPs@SEE): Optimization and assessment of photocatalytic degradation of methyl orange and their in vitro antibacterial and anticancer activity. Arab J Chem. 2022; 15: 103525.2